CrystEngComm

ROYAL SOCIETY OF CHEMISTRY

PAPER

View Article Online
View Journal | View Issue

Cite this: *CrystEngComm*, 2020, **22**, 2675

Ultrafast room-temperature synthesis of hierarchically porous metal–organic frameworks with high space–time yields†

Chongxiong Duan, [a] Yi Yu,[b] Feier Li,[b] Ying Wu*[b] and Hongxia Xi*[b]

Received 23rd October 2019,
Accepted 5th March 2020

DOI: 10.1039/c9ce01676g

rsc.li/crystengcomm

We developed a facile and general method to synthesize various HP-MOFs such as HKUST-1, ZIF-8, ZIF-61, and ZIF-90 within 1 min at room temperature and ambient pressure, using organic amines as protonation-templating agents. The morphology and porosity of hierarchically porous HKUST-1 can be readily tuned by varying the type of organic amines or the synthesis time. The space–time yield reached as high as 4.05×10^4 kg m^{-3} d^{-1}, at least 1 order of magnitude higher than previously reported values. In addition, the mechanism for rapid HP-MOF synthesis was elucidated for the first time by using a simulation technique. This strategy provides a new method for the facile, quick and large-scale synthesis of various HP-MOFs for a wide range of applications.

Introduction

Metal–organic frameworks (MOFs) or porous coordination polymers (PCPs), an interesting class of porous crystalline materials with a high surface area and permanent porosity,[1,2] have attracted considerable attention for potential industrial applications, including adsorption/separation,[3–5] drug delivery,[6] sensing,[7] and catalysis.[8] However, large-scale industrial application of MOFs faces two major challenges. First of all, almost all MOFs reported so far possess only micropores (pore size < 2 nm).[9] Thus, they can only be used with small molecules, as large reactant/product molecules cannot easily approach/leave the active sites in the internal pore channels of MOFs.[10] The second obstacle is the energy and time consumption during their synthesis (*e.g.*, commonly *via* solvothermal synthesis at high temperature and pressure (HTP) over 12 h),[11–13] with the space–time yield (STY) usually below 300 kg m^{-3} d^{-1}.[14] This increases the cost of their large-scale industrial production and commercial application.[15,16]

In response, many strategies have been developed to synthesize hierarchically porous MOFs (HP-MOFs) with micro- and mesopores (or micro-, meso- and macropores), including ligand-extension,[17] mixed-ligand,[18] post-processing,[19] and template methods.[20] However, these approaches still usually require excessive energy consumption (*e.g.*, HTP) and long reaction times (>12 h with low production rates).[21] A few specific approaches, such as microwave-assisted,[22] mechanochemical,[23] and sonochemical synthesis techniques,[24] have been used to reduce the energy consumption and improve the production rates of MOFs. Nevertheless, they often require complex apparatus, and more importantly, are still limited to microporous MOFs.[25,26] Therefore, the development of facile and efficient route for the rapid room-temperature synthesis of HP-MOFs is still a formidable challenge.

Herein, we developed a facile and general method to rapidly synthesize various HP-MOFs (HKUST-1, ZIF-8, ZIF-61, and ZIF-90) at room temperature, by employing organic amines as protonation-templating agents. The morphology and porosity of MOFs are easily tunable by varying the type of organic amines or the synthesis time. The space–time yield (STY) of hierarchically porous HKUST-1 was up to 4.05×10^4 kg m^{-3} d^{-1}, at least 10 times higher than previously reported values.[14,27] In addition, the role of organic amines in this rapid synthesis was disclosed based on a simulation method, in which the organic amines play two roles during synthesis as both protonation agents and templating agents.

Experimental

In the typical synthesis,[28] 1,3,5-benzenetricarboxylic acid (H_3BTC) in methanol solution was added to a $Cu(NO_3)_2$ aqueous solution at room temperature to form a transparent pale blue solution (ESI†). Glaucous floccules were immediately generated upon adding an organic amine (*N*,*N*,*N*,*N*-tetramethyl-1,6-hexanediamine, Table S1†), indicating the formation of HKUST-1. The cloudy solution was stirred for a given reaction time *t*, and the resulting glaucous precipitate

[a] *School of Materials Science and Energy Engineering, Foshan University, Foshan 528231, P. R. China*
[b] *School of Chemistry and Chemical Engineering, South China University of Technology, Guangzhou 510640, P. R. China. E-mail: w.y31@mail.scut.edu.cn, cehxxi@scut.edu.cn*

† Electronic supplementary information (ESI) available: More details of experimental and characterization processes. See DOI: 10.1039/c9ce01676g

was filtered, washed, activated and then dried. The products were denoted as HKUST-1_A*t* (*t* = 1, 10, or 30). The other three hierarchically porous MOFs (ZIF-8_A1, ZIF-61_A1, and ZIF-90_A1) were similarly synthesized within 1 min with *N*,*N*,*N*,*N*-tetramethyl-1,6-hexanediamine as the protonation-templating agent. In addition, the procedure used to synthesize HKUST-1_B1 was similar to the procedure used to prepare HKUST-1_A1, except that *N*,*N*,*N*,*N*-tetramethyl-1,6-hexanediamine was replaced with diethanolamine (see the ESI† for details).

Results and discussion

The experimental X-ray diffraction (XRD) patterns of the rapidly synthesized MOFs (HKUST-1_A1, ZIF-8_A1, ZIF-61_A1, and ZIF-90_A1) agree well with their corresponding simulated single-crystal data (Fig. 1), indicating the successful synthesis of MOF crystals at room temperature with a much reduced synthesis time (1 min) by using organic amines. Some peaks for the resulting MOFs are broader than those of the simulation data, likely due to either their small crystallite size or abundant lattice defects.[29,30] All the as-synthesized MOFs showed additional reflection peaks, suggesting other unidentified phases present in the materials. It should be noted that while the conventional synthesis requires long crystallization time,[14] our strategy could finish the synthesis within 1 min. This is consistent with previous reports that demonstrate that organic amines act as protonation agents to accelerate the formation of MOFs.[25,31,32]

The crystal morphologies of the four MOF products were revealed by electron microscopy. The scanning electron microscopy (SEM) image in Fig. 2a shows numerous vermiform mesopores uniformly distributed on the octahedral crystal surface of HKUST-1_A1, indicating that the mesoporosity of the material is derived from the textural crystal. The particle size was 500 ± 100 nm according to the transmission electron microscopy (TEM) image (Fig. 2b). The SEM image of ZIF-8_A1 (Fig. 2c) shows a dense, uniform

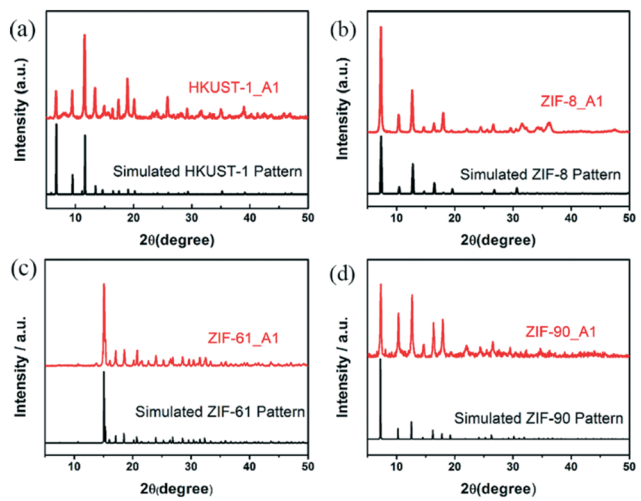

Fig. 1 Powder XRD patterns of the as-synthesized MOFs (red) and their simulated single-crystal data (black).

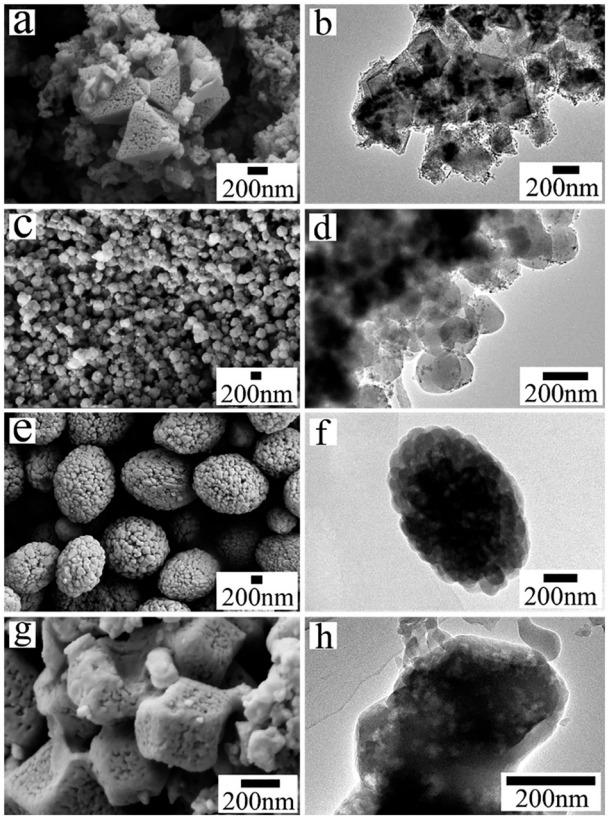

Fig. 2 SEM and TEM images of the hierarchically porous MOFs: (a and b) HKUST-1_A1; (c and d) ZIF-8_A1; (e and f) ZIF-61_A1; (g and h) ZIF-90_A1.

rhombic dodecahedral structure about 50 nm in diameter, with clear interparticle voids. In the corresponding TEM image (Fig. 2d), ZIF-8_A1 exhibits crowded nanoparticles of ~50 nm in diameter. These pores are randomly stacked to form abundant porous channels, with pore sizes of 12–100 nm according to the pore size distribution (PSD, Fig. S1a†). In the SEM image (Fig. 2e), ZIF-61_A1 has a massive olive-shaped morphology with a particle size of about 1–2 μm. Hierarchically porous phases with pore sizes of 15–200 nm exist between these aggregated nanoparticles, as shown in the PSD (Fig. S1b†) and TEM image (Fig. 2f). The SEM image in Fig. 2g shows that ZIF-90_A1 is composed of defective cube-shaped crystals, about 300 nm in size, and abundant pore voids (revealed by PSD to be ~18 nm in size, Fig. S1c†) are uniformly distributed on the crystal surface (Fig. 2h). These SEM observations agree well with the respective TEM images (Fig. 2b, d, f and h). In addition, the N_2 adsorption–desorption isotherms of ZIF-8_A1, ZIF-61_A1, and ZIF-90_A1 indicate the presence of mesopores, as shown in Fig. S2.† Overall, all four as-synthesized MOFs exhibit extended meso- and macroporous structures, most likely formed due to the introduced organic amines serving as the templates.[33]

To confirm the role of organic amines, one representative MOF (HKUST-1) was also synthesized using another organic amine (diethanolamine, Table S1†) as the protonation-templating agent, and the product is named HKUST-1_B1.

Compared to the octahedral structure of HKUST-1_A1 (Fig. 2a), the SEM image of HKUST-1_B1 (Fig. S3a†) exhibited defective octahedral crystals (structural defects) with serried and disordered stacking. This agrees with the observed broader XRD peaks (Fig. S4†). These structural defects can be related to fast crystal growth.[34] Moreover, the TEM image (Fig. S3b†) shows abundant porous channels between the HKUST-1_B1 particles, while the HKUST-1_A1 crystals are mesoporous themselves (Fig. 2a). In other words, the mesopores of HKUST-1_B1 primarily formed in the inter-particle voids. Such difference in porosity between HKUST-1_A1 and HKUST-1_B1 was also confirmed by the PSD data (Fig. S5†). From these results, both the crystal morphology and pore size of hierarchically porous HKUST-1 can be influenced by the type of organic amines. It should be noted from Fig. S5a† that, besides the intrinsic micropores of 0.8–0.9 nm, HKUST-1_X1 (X = A, B) also exhibited both meso- and macropores, which do not appear in conventional HKUST-1 (C-HKUST-1).[28] Although MOFs with both micro- and mesopores have been reported,[35] hierarchically porous HKUST-1 with pore diameters spanning all three ranges (micro-, meso- and macropores) has not been reported, to the best of our knowledge. In addition, the pore sizes of the as-synthesized MOFs depend on the size of the protonation-templating agent (Table S1 and Fig. S5†), which allows the control of the porosity properties of the MOFs. Thermogravimetric analysis (TGA) revealed that the hierarchically porous HKUST-1_X1 had a similar weight alteration curve to that of C-HKUST-1 during the same thermal treatment (Fig. S6†). It meant that the thermal stability of the rapidly synthesized hierarchically porous MOFs remained high. In addition, the introduction of mesopores and/or macropores does not decrease the thermal stability of hierarchically porous ZIFs (ZIF-8_A1, ZIF-61_A1, and ZIF-90_A1), and similar conclusions were drawn in earlier works of Fan *et al.*[36] and Li *et al.*[37] Elemental analysis showed that the prepared HKUST-1_X1 (X = A and B) samples contain some template residues, since the N element content of the organic amine is below 1.40% (Table S2†).

The synthesis time also affects the morphology and porosity of hierarchically porous HKUST-1_A*t*. The SEM and TEM images (Fig. 3) for t = 1, 10, and 30 are only slightly different from each other. HKUST-1_A1 shows an octahedral structure (Fig. 3a and d), while HKUST-1_A10 and HKUST-1_A30 show some nanosheet formation and more vermiform holes on the crystal surface (Fig. 3b and c). The TEM images (Fig. 3e and f) exhibit that the crystals are surrounded by a few nanosheets. The samples also differ slightly in the XRD peak intensity and width (Fig. S7†). Therefore, the synthesis time also affects the crystal morphology of these MOFs. To understand the detailed mechanism, the HKUST-1_A*t* samples were further evaluated by N_2 adsorption–desorption isotherms (Fig. 4a) and PSD (Fig. 4b). All three samples exhibited type IV isotherms (N_2 adsorption capacity >500 $cm^3\ g^{-1}$) with a wide hysteresis loop (type H4), suggesting the presence of abundant micropores and well-developed slit-shaped mesopores,[38,39] consistent with the SEM and TEM observations of vermiform pores (Fig. 3). From Fig. 4b, all the HKUST-1_A*t* samples possessed hierarchically porous structures constructed from micro-, meso-, and macropores. Moreover, when the synthesis time was increased from 1 to 30 min, the mesopores became more ordered, according to the PSD peak intensity (inset of Fig. 4b). This can be attributed to the more ordered arrays of organic amine molecules with extended stirring time.[35] These results confirm that synthesis time affects the morphology and porosity of HP-MOFs using a protonation-templating agent strategy.

The porosity properties, yield, and STY of the different HKUST-1 samples are summarized in Table 1. HKUST-1_A*t* and HKUST-1_B1 show a much higher total pore volume (V_t), mesopore volume (V_{meso}), and mesopore surface area (S_{meso}) than those of C-HKUST-1. The V_t of HKUST-1_A*t* increased from 0.61 to 0.74 $cm^3\ g^{-1}$ with the synthesis time (t) increased from 1 to 30 min, and the V_{meso} value also increased from 0.34 to 0.44 $cm^3\ g^{-1}$ in accordance with the PSD results (Fig. 4b). More importantly, the yields of HKUST-1_X*t* are much higher than that of C-HKUST-1. The STY of HKUST-1_A1 is up to 4.05×10^4 kg $m^{-3}\ d^{-1}$, about 19 times the highest reported STY for mesoporous HKUST-1 (2035 kg $m^{-3}\ d^{-1}$),[27] and is even higher than the record for C-HKUST-1 (3.6×10^4 kg $m^{-3}\ d^{-1}$) synthesized with hydroxy double salts (HDSs).[40] It is also over two orders of magnitude higher than that of

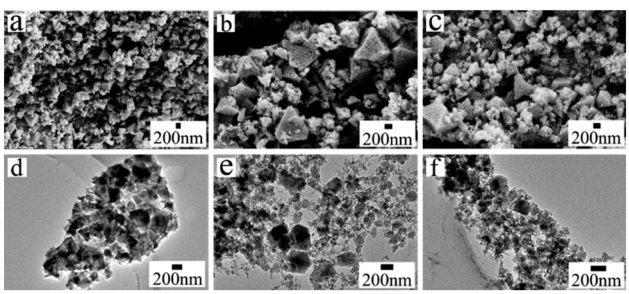

Fig. 3 SEM and TEM images of the hierarchically porous HKUST-1_A*t* samples produced at different synthesis times: (a and d) HKUST-1_A1; (b and e) HKUST-1_A10; (c and f) HKUST-1_A30.

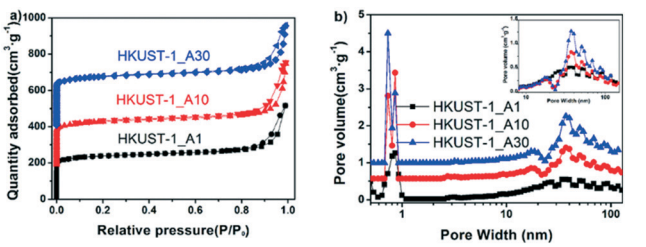

Fig. 4 (a) N_2 adsorption–desorption isotherms of the hierarchically porous HKUST-1_A*t* (t = 1, 10, 30) samples. For clarity, isotherms of the HKUST-1_A10 and HKUST-1_A30 samples are offset by −190 and −400 $cm^3\ g^{-1}$, respectively. (b) The pore size distribution (PSD) curves of the hierarchically porous HKUST-1_A*t* (t = 1, 10, 30) samples. For clarity, isotherms of the HKUST-1_A1–HKUST-1_A30 samples are vertical offset by −0.02, −0.5 and −1.0 $cm^3\ g^{-1}$, respectively.

Table 1 Porosity properties, STY and yield of C-HKUST-1 and the HKUST-1_X*t* samples synthesized in this work

Sample	S_{BET}[a] [$m^2\ g^{-1}$]	S_{meso}[b] [$m^2\ g^{-1}$]	V_t[c] [$cm^3\ g^{-1}$]	V_{meso}[d] [$cm^3\ g^{-1}$]	STY[e] [$kg\ m^{-3}\ d^{-1}$]	Yield[f]
C-HKUST-1	1328	116	0.60	0.05	37	78%
HKUST-1_A1	916	193	0.61	0.34	4.05×10^4	87%
HKUST-1_A10	977	228	0.73	0.43	4.12×10^3	90%
HKUST-1_A30	1037	240	0.74	0.44	1.48×10^3	96%
HKUST-1_B1	1063	222	0.67	0.31	3.6×10^4	81%

[a] S_{BET}: Brunauer–Emmett–Teller (BET) surface area. [b] S_{meso}: mesopore surface area calculated using the BET equation. [c] V_t: total pore volume. [d] V_{meso}: mesopore volume based on non-local density functional theory (NLDFT) calculations. [e] STY: calculated from the mass of active products. [f] Yield: isolated yield.

commercial HKUST-1 (Basolite C300, 225 kg m^{-3} d^{-1}).[41] In addition, the as-synthesized ZIF materials have high space–time yields (Table S3†), which are comparable to the space–time yields of Al-MOFs with ton-scale production.[42] Therefore, the use of protonation-templating agents under mild conditions has enormous potential for scaled-up production of hierarchically porous MOFs.

Fig. 5 shows the molecular electrostatic potential (MEP) map and the highest occupied molecular orbital (HOMO) of the organic amine (*N*,*N*,*N*,*N*-tetramethyl-1,6-hexanediamine). The region with negative MEP (red) is related to electrophilic reactivity, and the positive one (blue) to nucleophilic reactivity.[43] As observed in Fig. 5a, the negative region is mainly focused on the amine group, which is the most susceptible site for electrophilic attacks.[44,45] The HOMO is directly related to the ionization potential and characterizes the susceptibility of a molecule to attack by electrophiles.[46] It was observed from Fig. 5b that the HOMO is also mainly located on the amine group. The other organic amine (diethanolamine) showed a similar MEP and HOMO (Fig. S8†). From these results, the amine group of the organic amines is easily attacked by electrophilic species. Therefore, the organic amines played the role of protonation agents mainly due to the function of the amine group. Furthermore, to investigate the underlying formation mechanism of hierarchical pores, we performed DFT calculations using DMol3 to simulate the minimum energy path.[47] In the calculations, the GGA-PBE level with DNP basis set of complete LST/QST protocol was adopted, and the Grimme method was performed for DFT-D corrections,[48] while the RMS convergence was set to 0.002 Ha $Å^{-1}$. As shown in Fig. 6, the ligand captured by the organic amine exhibits a transition state with an activation barrier of 0.79 eV, and such a barrier is prone to be overcome at room temperature during the synthesis process.

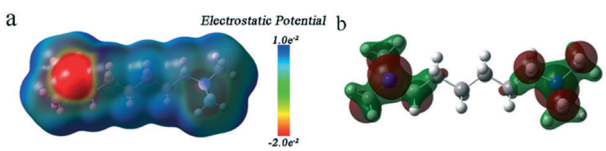

Fig. 5 (a) Molecular electrostatic potential map (MEP); (b) molecular orbital surfaces of *N*,*N*,*N*,*N*-tetramethyl-1,6-hexanediamine (white ball = hydrogen atom; gray ball = carbon atom; blue ball = nitrogen atom).

The connection between the ligands through Cu ions shows a much smoother energy profile (negligible barrier), which indicates a spontaneous step due to the H atoms of the ligands having been taken by the organic amine, leaving available oxygen sites for bond formation. It seems that the rate-determining step is at the end of the process, requiring 13.74 eV of activation energy to separate the organic amines from the structure and form mesopores. Thus, we experimentally applied a temperature of 333 K for this step to overcome the barrier, and successfully eliminated the organic amines from the material.

The influence of the pH value on the MOF synthesis was investigated in detail. When the pH is below 6.0 (acidic system), the as-synthesized products showed poor crystallinity and porosity, as confirmed by XRD (Fig. S9†), N_2 adsorption–desorption and pore size distribution data (Fig. S10†), respectively. When the pH was adjusted to alkaline conditions, such as 8.2 and 8.6, the HKUST-1 crystals could not be obtained, as confirmed by XRD (Fig. S9†). These results indicate that alkaline conditions are unfavorable to the formation of the HKUST-1 crystals. Based on these results, *N*,*N*,*N*,*N*-tetramethyl-1,6-hexanediamine and diethanolamine are believed to play two roles during synthesis: (1) as protonation

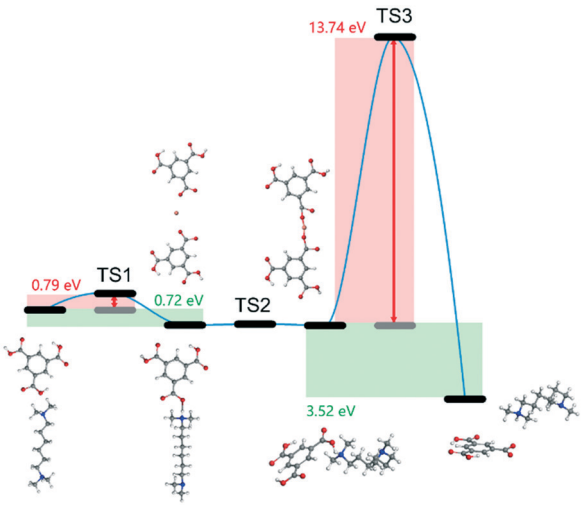

Fig. 6 Minimum energy path for hierarchically porous MOF synthesis with the corresponding intermediates and transition states, calculated at the GGA-PBE level.

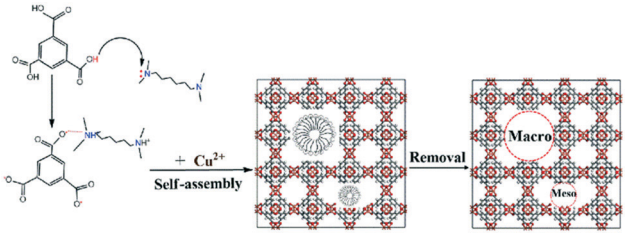

Scheme 1 Schematic diagram of the ultrafast room-temperature preparation of hierarchically porous MOFs.

agents that deprotonate the H_3BTC ligand and accelerate the formation of MOF crystals,[25,31,35] and (2) as templating agents that direct the formation of meso/macropores.[35,49] A possible mechanism for the rapid fabrication of hierarchically porous MOFs is illustrated in Scheme 1. First, the amine headgroup of *N*,*N*,*N*,*N*-tetramethyl-1,6-hexanediamine or diethanolamine has a strong interaction with the hydrogen in H_3BTC, causing the H_3BTC ligand to lose protons and form BTC^{3-}, a key step for the rapid formation of MOF crystals.[25,31,35] Subsequently, the metal ion (Cu^{2+}) interacts with BTC^{3-} to self-assemble quickly on the surface of the template molecules.[35,49] Finally, the *N*,*N*,*N*,*N*-tetramethyl-1,6-hexanediamine or diethanolamine molecules are removed to yield meso/macropores with walls formed by crystalline microporous MOFs.[50,51]

Conclusions

In summary, we report a facile and general approach to rapidly synthesize four hierarchically porous MOFs (HKUST-1, ZIF-8, ZIF-61, and ZIF-90) under ambient conditions. The synthesis time can be as short as 1 min, and the resulting MOF products all had hierarchically porous structures with micro-, meso-, and macropores. The morphology and porosity of the prepared HKUST-1 can also be easily tuned by changing the type of organic amines or the synthesis time. The maximum STY (4.05×10^4 kg m^{-3} d^{-1}) is at least 1 order of magnitude higher than any previously reported values for hierarchically porous MOFs. The organic amines play two roles during the synthesis: (1) as protonation agents that deprotonate the organic ligands and accelerate the formation of MOF crystals, and (2) as templating agents that direct the formation of meso/macropores. Due to the fast diffusion and transfer of large molecules through the meso/macropores, the hierarchically porous HKUST-1 exhibited considerably higher catalytic activity for reactions involving large molecules compared to conventional HKUST-1 containing only micropores. The protonation-templating agent strategy developed in this work is very promising for the large-scale industrial synthesis of diverse hierarchically porous MOFs as catalysts for reactions involving large molecules.

Conflicts of interest

The authors declare no competing financial interest.

Acknowledgements

We gratefully acknowledge the financial support from the National Natural Science Foundation of China (21576094 and 21808067), the Guangdong Natural Science Foundation (2017A030313052), the China Postdoctoral Science Foundation (2018M640785), and the Fundamental Research Funds for the Central Universities (2018MS86).

Notes and references

1 S. Abednatanzi, P. Gohari Derakhshandeh, H. Depauw, F.-X. Coudert, H. Vrielinck, P. Van Der Voort and K. Leus, *Chem. Soc. Rev.*, 2019, **48**, 2535–2565.
2 Q. Qiu, H. Chen, Y. Wang and Y. Ying, *Coord. Chem. Rev.*, 2019, **387**, 60–78.
3 C. Duan, F. Li, M. Yang, H. Zhang, Y. Wu and H. Xi, *Ind. Eng. Chem. Res.*, 2018, **57**, 15385–15394.
4 Y. Qiu, S. Zhang, D. Cui, M. Li, J. Zeng, D. Zeng and R. Xiao, *Appl. Energy*, 2019, **252**, 113454.
5 B. Tan, Y. Luo, X. Liang, S. Wang, X. Gao, Z. Zhang and Y. Fang, *Ind. Eng. Chem. Res.*, 2019, **58**, 15712–15720.
6 A. C. McKinlay, R. E. Morris, P. Horcajada, G. Férey, R. Gref, P. Couvreur and C. Serre, *Angew. Chem., Int. Ed.*, 2010, **49**, 6260–6266.
7 L. E. Kreno, K. Leong, O. K. Farha, M. Allendorf, R. P. Van Duyne and J. T. Hupp, *Chem. Rev.*, 2011, **112**, 1105–1125.
8 F. Li, K. Zheng, H. Zhang, C. Duan and H. Xi, *ACS Sustainable Chem. Eng.*, 2019, **7**, 11080–11087.
9 W. Xuan, C. Zhu, Y. Liu and Y. Cui, *Chem. Soc. Rev.*, 2012, **41**, 1677–1695.
10 C. Duan, J. Huo, F. Li, M. Yang and H. Xi, *J. Mater. Sci.*, 2018, **53**, 16276–16287.
11 C. Duan, F. Li, H. Zhang, J. Li, X. Wang and H. Xi, *RSC Adv.*, 2017, **7**, 52245–52251.
12 D. Yuan, M. Sun, S. Tang, Y. Zhang, Z. Wang, J. Qi, Y. Rao and Q. Zhang, *Chin. Chem. Lett.*, 2020, **31**, 547–550.
13 C. Duan, Y. Yu, J. Xiao, X. Zhang, L. Li, P. Yang, J. Wu and H. Xi, *Sci. China Mater.*, 2020, DOI: 10.1007/s40843-019-1264-x.
14 N. Stock and S. Biswas, *Chem. Rev.*, 2012, **112**, 933–969.
15 D. Zeng, Y. Qiu, S. Peng, C. Chen, J. Zeng, S. Zhang and R. Xiao, *J. Mater. Chem. A*, 2018, **6**, 11306–11316.
16 K. Wang, L. Li, Y. Lan, P. Dong and G. Xia, *Math. Probl. Eng.*, 2019, 1–8.
17 V. Lykourinou, Y. Chen, X.-S. Wang, L. Meng, T. Hoang, L.-J. Ming, R. L. Musselman and S. Ma, *J. Am. Chem. Soc.*, 2011, **133**, 10382–10385.
18 C. Duan, Y. Yu, P. Yang, X. Zhang, F. Li, L. Li and H. Xi, *Ind. Eng. Chem. Res.*, 2020, **59**, 774–782.
19 Y. Kim, T. Yang, G. Yun, M. B. Ghasemian, J. Koo, E. Lee, S. J. Cho and K. Kim, *Angew. Chem., Int. Ed.*, 2015, **54**, 13273–13278.
20 C. Duan, F. Li, J. Xiao, Z. Liu, C. Li and H. Xi, *Sci. China Mater.*, 2017, **60**, 1205–1214.

21 B. Tan, Y. Luo, X. Liang, S. Wang, X. Gao, Z. Zhang and Y. Fang, *Ind. Eng. Chem. Res.*, 2019, **58**, 2983–2990.
22 Z. Ni and R. I. Masel, *J. Am. Chem. Soc.*, 2006, **128**, 12394–12395.
23 P. J. Beldon, L. Fábián, R. S. Stein, A. Thirumurugan, A. K. Cheetham and T. Friščić, *Angew. Chem., Int. Ed.*, 2010, **49**, 9640–9643.
24 H.-Y. Cho, J. Kim, S.-N. Kim and W.-S. Ahn, *Microporous Mesoporous Mater.*, 2013, **169**, 180–184.
25 J.-L. Zhuang, D. Ceglarek, S. Pethuraj and A. Terfort, *Adv. Funct. Mater.*, 2011, **21**, 1442–1447.
26 J. Wu, K. Yin, M. Li, Z. Wu, S. Xiao, H. Wang, J.-A. Duan and J. He, *Nanoscale*, 2020, **12**, 4077–4084.
27 J. Huo, M. Brightwell, S. El Hankari, A. Garai and D. Bradshaw, *J. Mater. Chem. A*, 2013, **1**, 15220–15223.
28 S. S.-Y. Chui, S. M.-F. Lo, J. P. Charmant, A. G. Orpen and I. D. Williams, *Science*, 1999, **283**, 1148–1150.
29 T. Ungár, *Scr. Mater.*, 2004, **51**, 777–781.
30 Q. Bao, Y. Lou, T. Xing and J. Chen, *Inorg. Chem. Commun.*, 2013, **37**, 170–173.
31 D. J. Tranchemontagne, J. R. Hunt and O. M. Yaghi, *Tetrahedron*, 2008, **64**, 8553–8557.
32 Y. Pan, Y. Liu, G. Zeng, L. Zhao and Z. Lai, *Chem. Commun.*, 2011, **47**, 2071–2073.
33 V. Guillerm, D. Kim, J. F. Eubank, R. Luebke, X. Liu, K. Adil, M. S. Lah and M. Eddaoudi, *Chem. Soc. Rev.*, 2014, **43**, 6141–6172.
34 G. Bhagavannarayana, P. Rajesh and P. Ramasamy, *J. Appl. Crystallogr.*, 2010, **43**, 1372–1376.
35 D. Bradshaw, S. El-Hankari and L. Lupica-Spagnolo, *Chem. Soc. Rev.*, 2014, **43**, 5431–5443.
36 S. Wang, Y. Fan and X. Jia, *Chem. Eng. J.*, 2014, **256**, 14–22.
37 Y.-n. Wu, M. Zhou, B. Zhang, B. Wu, J. Li, J. Qiao, X. Guan and F. Li, *Nanoscale*, 2014, **6**, 1105–1112.
38 W.-H. Zhang, J.-L. Shi, L.-Z. Wang and D.-S. Yan, *Chem. Mater.*, 2000, **12**, 1408–1413.
39 K. S. Sing, *Pure Appl. Chem.*, 1985, **57**, 603–619.
40 J. Zhao, W. T. Nunn, P. C. Lemaire, Y. Lin, M. D. Dickey, C. J. Oldham, H. J. Walls, G. W. Peterson, M. D. Losego and G. N. Parsons, *J. Am. Chem. Soc.*, 2015, **137**, 13756–13759.
41 A. U. Czaja, N. Trukhan and U. Muller, *Chem. Soc. Rev.*, 2009, **38**, 1284–1293.
42 M. Gaab, N. Trukhan, S. Maurer, R. Gummaraju and U. Müller, *Microporous Mesoporous Mater.*, 2012, **157**, 131–136.
43 C. Duan, F. Li, S. Luo, J. Xiao, L. Li and H. Xi, *Chem. Eng. J.*, 2018, **334**, 1477–1483.
44 N. Okulik and A. H. Jubert, *Internet Electron. J. Mol. Des.*, 2005, **4**, 17–30.
45 F. Li, C. Duan, H. Zhang, X. Yan, J. Li and H. Xi, *Ind. Eng. Chem. Res.*, 2018, **57**, 9136–9143.
46 K. F. Khaled, S. A. Fadl-Allah and B. Hammouti, *Mater. Chem. Phys.*, 2009, **117**, 148–155.
47 B. Delley, *J. Chem. Phys.*, 2000, **113**, 7756–7764.
48 S. Grimme, *J. Comput. Chem.*, 2006, **27**, 1787–1799.
49 L. G. Qiu, T. Xu, Z. Q. Li, W. Wang, Y. Wu, X. Jiang, X. Y. Tian and L. D. Zhang, *Angew. Chem., Int. Ed.*, 2008, **47**, 9487–9491.
50 L.-B. Sun, J.-R. Li, J. Park and H.-C. Zhou, *J. Am. Chem. Soc.*, 2011, **134**, 126–129.
51 H. Zhang, J. Huo, J. Li, F. Li, C. Duan and H. Xi, *CrystEngComm*, 2018, **20**, 5754–5759.

